Eur. Phys. J. C 24, 425–437 (2002)
Digital Object Identifier (DOI) 10.1007/s10052-002-0957-3

THE EUROPEAN PHYSICAL JOURNAL C

A phenomenological interpretation of open charm production at HERA in terms of the semi-hard approach

S.P. Baranov[1,a], H. Jung[2,b], L. Jönsson[2,c], S. Padhi[3,d], N.P. Zotov[4,e]

[1] Lebedev Institute of Physics, Leninsky prosp. 53, Moscow 117924, Russia
[2] Department of Elementary Particle Physics, Lund University, 22100 Lund, Sweden
[3] Department of Physics, McGill University, Montreal, Quebec H3A 2T8, Canada
[4] Skobeltsyn Institute of Nuclear Physics, Moscow State University, Moscow 119992, Russia

Received: 4 March 2002 /
Published online: 7 June 2002 –

Abstract. In the framework of the semi-hard (k_t-factorization) approach, we analyze the various charm production processes in the kinematic region covered by the HERA experiments.

1 Introduction

At the energies of modern lepton–hadron and hadron–hadron colliders, the interaction dynamics is governed by the properties of parton distributions in the small x region. This domain is characterized by the double inequality $s \gg \mu^2 \gg \Lambda^2$, which shows that the typical parton interaction scale μ is much higher than the QCD parameter Λ, but is much lower than the total c.m.s. energy $s^{1/2}$. The situation is therefore classified as "semi-hard". In such a case, the perturbative QCD expansions in α_s may contain large coefficients $\mathcal{O}\left[\log(s/\mu^2)\right] = \mathcal{O}\left[\log(1/x)\right]$ which compensate the smallness of the coupling constant $\alpha_s(\mu^2/\Lambda^2)$. The resummation [1,2] of the terms $\left[\log(1/x)\alpha_s\right]^n$ results in the so-called unintegrated parton distribution $\mathcal{F}(x,k_t^2)$, which determines the probability to find a parton carrying the longitudinal momentum fraction x and transverse momentum k_t. If the terms $\left[\log(\mu^2/\Lambda^2)\alpha_s\right]^n$ and $\left[\log(\mu^2/\Lambda^2)\log(1/x)\alpha_s\right]^n$ are also resummed, then the unintegrated parton distribution depends also on the probing scale μ; it will be labeled $\mathcal{A}(x,k_t^2,\mu^2)$. That generalizes the factorization of the hadronic matrix elements beyond the collinear approximation (hereafter this generalized factorization will be referred to as "k_t-factorization" [2,3]). The unintegrated parton distributions obey certain evolution equations (e.g., BFKL [4–6] or CCFM [7–10]) and are related to the conventional DGLAP [11–14] densities once the k_t dependence is integrated out. Nowadays, the significance of the k_t-factorization (semi-hard) approach becomes more and more commonly recognized. Its applications to a variety of photo-, lepto- and hadro-production processes are widely discussed in the literature [15–32]. Remarkable agreement is found between the data and the theoretical calculations regarding photo- [20] and electroproduction [21,22] of D^* mesons, and of forward jets [23, 24], as well as for specific kinematic correlations observed in photo-production of D^* mesons associated with jets [25] at HERA. Also in hadro-production of beauty [26–28], χ_c [29] and J/ψ [30–32] at the TEVATRON good agreement is observed. However, for a consistent application of k_t-factorization in different models, the unintegrated gluon distribution has to be determined in the same framework. Also the various approximations needed to describe the experimental data have to be carefully investigated. In the present paper we have attempted a systematic comparison of model predictions with experimental data regarding the heavy flavor production processes at HERA.

2 The k_t-factorization approach applied to charm production

The production of open-flavored $c\bar{c}$ pairs in ep-collisions is described in terms of the photon–gluon fusion mechanism. A generalization of the usual parton model to the k_t-factorization approach implies two essential steps. These are the introduction of unintegrated gluon distributions and the modification of the gluon spin density matrix in the parton-level matrix elements.

Here we consider only $\gamma^* g^* \to c\bar{c}$. Let k_γ, k_g, p_c and $p_{\bar{c}}$ be the four-momenta of the initial state photon, the initial state gluon, the final state quark and antiquark respectively, and ϵ_γ and ϵ_g are the corresponding polarization vectors. The photon–gluon fusion matrix elements for the production of an open-flavored $c\bar{c}$ pair then reads (with a charm mass m_c):

[a] e-mail: baranov@sci.lebedev.ru
[b] e-mail: jung@mail.desy.de
[c] e-mail: leif@quark.lu.se
[d] e-mail: Sanjay.Padhi@desy.de
[e] e-mail: zotov@theory.sinp.msu.ru

Table 1. Comparison of different calculations of the matrix elements for $\gamma^* g^* \to c\bar{c}$. Shown are the matrix elements normalized to the matrix element CE-CCH for $p_{\mathrm{t}c} = 5\,\mathrm{GeV}$, $\eta_c = \eta_{\bar{c}} = 0$ in the ep c.m.s. with $s^{1/2} = 300\,\mathrm{GeV}$. For the comparisons the momenta of the incoming and outgoing partons have been modified to satisfy the small x requirement: $k_\gamma = x_\gamma p_e + \vec{k}_{\mathrm{t}\gamma}$ and $k_{\mathrm{g}} = x_{\mathrm{g}} p_p + \vec{k}_{\mathrm{t}}$ resulting in $k_\gamma^2 = -k_{\mathrm{t}\gamma}^2$ and $k_{\mathrm{g}}^2 = -k_{\mathrm{t}}^2$

	CE-CCH	SZ	BZ
$k_{\mathrm{t}\gamma} = k_{\mathrm{t}} = 0\,\mathrm{GeV}$	1	1	0.9
$k_{\mathrm{t}\gamma} = 0\,\mathrm{GeV}$, $k_{\mathrm{t}} = 10\,\mathrm{GeV}$	1	1	0.86
$k_{\mathrm{t}\gamma} = 10\,\mathrm{GeV}$, $k_{\mathrm{t}} = 0\,\mathrm{GeV}$	1	1	0.96
$k_{\mathrm{t}\gamma} = 10\,\mathrm{GeV}$, $k_{\mathrm{t}} = 10\,\mathrm{GeV}$	1	1	0.93

$$\mathcal{M}(\gamma g \to c\bar{c}) = \bar{u}(p_c)\left(\frac{\not\epsilon_\gamma(\not p_c - \not k_\gamma + m_c)\,\not\epsilon_{\mathrm{g}}}{k_\gamma^2 - 2k_\gamma p_c} + \frac{\not\epsilon_{\mathrm{g}}(\not p_c - \not k_g + m_c)\,\not\epsilon_\gamma}{k_g^2 - 2k_g p_c}\right) u(p_{\bar{c}}). \quad (1)$$

The matrix element squared for open heavy quark production has already been calculated in [2,3], which we label CE-CCH in the following. In [33] (labeled as SZ) the calculation of the matrix elements for open heavy quark production has been repeated. In [20,25] (labeled as BZ) the method of orthogonal amplitudes [34] was applied. When calculating the spin average of the matrix element squared, BZ uses $L^{\mu\nu}$ for the photon polarization matrix:

$$L^{\mu\nu} = \overline{\epsilon_\gamma^\mu \epsilon_\gamma^{*\nu}} = 4\pi\alpha\left[8p_e^\mu p_e^\nu - 4(p_e k_\gamma)g^{\mu\nu}\right]/(k_\gamma^2)^2, \quad (2)$$

where p_e is the four momentum of the incoming electron. This expression also includes the photon propagator factor and photon–lepton coupling. In the calculation of CE-CCH and SZ the photon is treated in a similar way as was the gluon in [2]:

$$G^{\mu\nu} = \overline{\epsilon_g^\mu \epsilon_g^{*\nu}} = k_{tg}^\mu k_{tg}^\nu / |k_{tg}|^2. \quad (3)$$

This formula converges to the usual $\sum \epsilon^\mu \epsilon^{*\nu} = -g^{\mu\nu}$ when $k_{\mathrm{t}} \to 0$.

In BZ the complete set of matrix elements have been tested for gauge invariance by substituting the gluon momenta with their polarization vectors showing explicitly the gauge invariance of the matrix element in order $\mathcal{O}(\alpha_{\mathrm{s}})$.

The hard scattering cross section for a boson–gluon fusion process is written as a convolution of the partonic cross section $\hat{\sigma}(x_g, k_{\mathrm{t}};\ \gamma^* g^* \to q\bar{q})$ with the k_{t} dependent (unintegrated) gluon density $\mathcal{A}(x, k_{\mathrm{t}}^2, \mu^2)$ (here and in the following k_{t} ($k_{\mathrm{t}\gamma}$) is a shorthand notation for $|\vec{k}_{\mathrm{t}}|$ ($|\vec{k}_{\mathrm{t}\gamma}|$) with $\vec{k}_{\mathrm{t}}$ ($\vec{k}_{\mathrm{t}\gamma}$) being the two-dimensional vector of the transverse momentum of the gluon (photon)):

$$\sigma = \int \mathrm{d}k_{\mathrm{t}}^2 \mathrm{d}x_g \mathcal{A}(x_g, k_{\mathrm{t}}^2, \mu^2)\hat{\sigma}(x_g, k_{\mathrm{t}};\ \gamma^* g^* \to q\bar{q}), \quad (4)$$

with the off-shell matrix elements either given by CE-CCH, SZ or by BZ. The multidimensional integrations can be performed by means of the Monte Carlo technique either by using VEGAS [35] for the pure parton-level calculations, or by using the full Monte Carlo event generator CASCADE [23,24,36]. Since it is difficult to compare the different matrix elements with each other analytically and to prove that they agree, we have performed several numerical checks. In Table 1 we show a numerical comparison of the different matrix elements for $\gamma^* g^* \to c\bar{c}$. For the comparison we have chosen the transverse momentum of the charm quark to be $p_{\mathrm{t}c} = 5\,\mathrm{GeV}$, its rapidity to be $\eta_c = \eta_{\bar{c}} = 0$ in the ep c.m.s., and we calculated the other kinematic quantities accordingly. The transverse momenta of the incoming partons are as indicated in the table. In addition we have removed all α_{s} dependencies from the matrix elements. In the calculation of the off-shell matrix elements, approximations are necessary to satisfy the k_{t}-factorization theorem: the gluon polarization tensor as given in (3) is applied (which is different from the full polarization tensor of (2)), and the transverse momentum must be dominating the virtuality: $k^2 = -k_{\mathrm{t}}^2$. The last condition is essentially the small x (or high energy) approximation. These criteria are satisfied in the calculations of CE-CCH and SZ, whereas the calculation of BZ is done using the full polarization tensor $L^{\mu\nu}$ for the photon and only $G^{\mu\nu}$ for the gluon without applying the small x approximation to the gluon four-vector. To study the effect of the different approximations, we have compared the matrix elements at large c.m.s energies of $s^{1/2} = 30\,000\,\mathrm{GeV}$ and observe good agreement for all cases. This means that in the asymptotic limit of very high energies the small x approximation and the use of $G^{\mu\nu}$ are justified. In Table 1 we compare the matrix elements at a c.m.s energy of $s^{1/2} = 300\,\mathrm{GeV}$, typical for HERA experiments, for different values of the transverse photon momentum $k_{\mathrm{t}\gamma}$ and the incoming gluon k_{t}. Whereas the calculations of CE-CCH and SZ agree perfectly in all cases, a systematic difference of the order of $\sim 10\%$ from the calculation of BZ is observed. Since we obtained agreement in the high energy limit, this can be attributed to the effect of the small x approximation. In addition BZ treat the polarization of the photon and the gluon differently, and therefore this effect can be quantified by observing a difference of $\sim 10\%$ between rows two and three in Table 1. The above investigations indicate that the effects of the small x approximation applied at HERA energies are of the order of $\sim 10\%$.

It is also interesting to consider the limit $k_{\mathrm{t}} \to 0$ of the matrix elements. To do that we define a reduced cross section $\tilde{\sigma}$:

$$\tilde{\sigma}(k_{\mathrm{t}}) = \int \mathrm{dLips}|\mathrm{ME}|^2, \quad (5)$$

where we integrate over the Lorentz-invariant phase space (Lips) of the final state quarks. The matrix element $|\mathrm{ME}|^2$ is taken from CE-CCH, where we have set $16\pi^2\alpha_{\mathrm{em}}\alpha_{\mathrm{s}}e_q^2 \equiv 1$. In Fig. 1 we show $\tilde{\sigma}(k_{\mathrm{t}})$ as a function of the transverse momentum of the incoming gluon k_{t} for quark masses of $m = 1.5\,\mathrm{GeV}$ in Fig. 1a and for $m = 5\,\mathrm{GeV}$ in Fig. 1b using $s^{1/2} = 30\,000\,\mathrm{GeV}$ and a fixed $x_\gamma = x_g = 0.01$. In both cases a smooth behavior for $k_{\mathrm{t}} \to 0$ is observed. It is

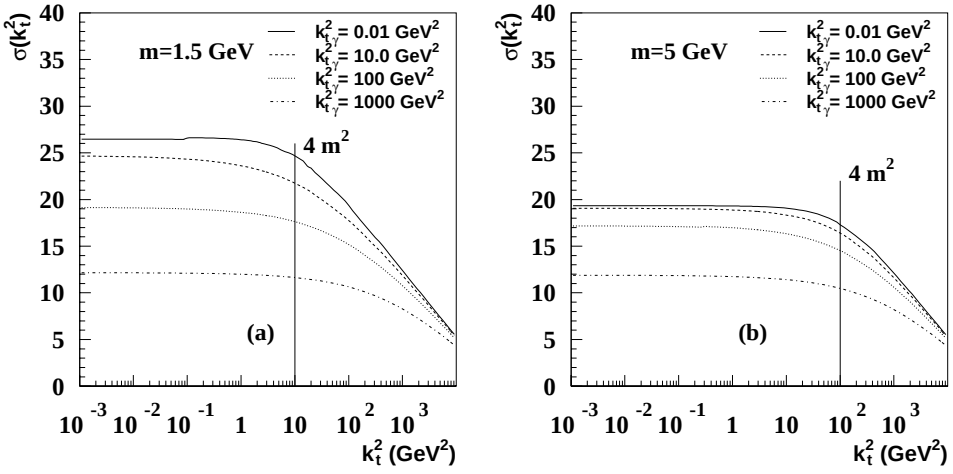

Fig. 1a,b. The reduced cross section $\tilde{\sigma}(k_t)$ as a function of the transverse momentum k_t of the incoming gluon for different values of the transverse momentum of the incoming photon $k_{t\gamma}$ ($m = 1.5\,\mathrm{GeV}$ in **a**, $m = 5\,\mathrm{GeV}$ in **b**, $s^{1/2} = 30\,000\,\mathrm{GeV}$ and a fixed $x_\gamma = x_g = 0.01$)

also interesting to note that in all cases the cross section starts to decrease at $k_t^2 \gtrsim 4m^2$. The region $k_t^2 > 4m^2$ is still contributing to the total cross section significantly, showing one of the main differences to the usual collinear approximation, where this region is completely ignored.

3 The unintegrated gluon distributions

Cross section calculations require an explicit representation of the k_t dependent (unintegrated) gluon density $\mathcal{A}(x, k_t^2, \mu^2)$. We have used three different representations, one (JB) coming from a leading-order perturbative solution of the BFKL equations [37], the second set (JS) derived from a numerical solution of the CCFM equation [23,24] and the third (KMR) from the solution of a combination of the BFKL and DGLAP equations [38].

JB

The unintegrated gluon density $\mathcal{A}(x, k_t^2, \mu^2)$, in the approach of [37], is calculated as a convolution of the ordinary gluon density $xG(x, \mu^2)$ (here we use GRV [39]) with universal weight factors:

$$\mathcal{A}(x, k_t^2, \mu^2) = \int_x^1 \mathcal{G}(z, k_t^2, \mu^2) \frac{x}{z} G\left(\frac{x}{z}, \mu^2\right) \mathrm{d}z, \quad (6)$$

$$\mathcal{G}(z, k_t^2, \mu^2) = \frac{\bar{\alpha}_s}{z k_t^2} J_0(2\sqrt{\bar{\alpha}_s \ln(1/z) \ln(\mu^2/k_t^2)}), \quad k_t^2 < \mu^2, \quad (7)$$

$$\mathcal{G}(z, k_t^2, \mu^2) = \frac{\bar{\alpha}_s}{z k_t^2} I_0(2\sqrt{\bar{\alpha}_s \ln(1/z) \ln(k_t^2/\mu^2)}), \quad k_t^2 > \mu^2, \quad (8)$$

where J_0 and I_0 stand for Bessel functions (of real and imaginary arguments, respectively), and $\bar{\alpha}_s = 3\alpha_s/\pi$ is connected to the pomeron intercept $\alpha(0) = 1 + \Delta$, with $\Delta = \bar{\alpha}_s 4 \log 2$ in LO. An expression for Δ in NLO is given in [40]: $\Delta = \bar{\alpha}_s 4 \log 2 - N\bar{\alpha}_s^2$. In our calculations presented here we use the solution of the LO BFKL equation and treat Δ as a free parameter varying between $0.166 < \Delta < 0.53$ with a central value of $\Delta = 0.35$.

JS

The CCFM evolution equations have been solved numerically in [23,24] using a Monte Carlo method. According to the CCFM evolution equation, the emission of partons during the initial cascade is only allowed in an angular-ordered region of phase space. The maximum allowed angle Ξ for any gluon emission sets the scale μ^2 for the evolution and is defined by the hard scattering quark box, which connects the exchanged gluon to the virtual photon.

The free parameters of the starting gluon distribution were fitted to the structure function $F_2(x, Q^2)$ in the range $x < 10^{-2}$ and $Q^2 > 5\,\mathrm{GeV}^2$ as described in [24].

KMR

In KMR [38] the dependence of the unintegrated gluon distribution on the two scales k_t^2 and μ^2 was investigated: the scale μ^2 plays a dual role: it acts as the factorization scale and also controls the angular ordering of the partons emitted in the evolution. This results in a form similar to the differential form of the CCFM equation, however the splitting function $P(z)$ is taken from the single scale evolution of the *unified* DGLAP-BFKL expression discussed in [41]. The unintegrated gluon density $x\mathcal{A}(x, k_t^2, \mu^2)$ covering the whole range in k_t^2 has been evaluated by [42], giving

$$x\mathcal{A}(x, k_t^2, \mu^2) = \begin{cases} \dfrac{xG(x, k_{t0}^2)}{k_{t0}^2} & \text{if} k_t < k_{t0}, \\ \dfrac{f(x, k_t^2, \mu^2)}{k_t^2} & \text{if } k_t \geq k_{t0}, \end{cases} \quad (9)$$

with $xG(x, k_{t0}^2)$ being the integrated MRST [43] gluon density function and $f(x, k_t^2, \mu^2)$ being the unintegrated gluon density of [38] starting from $k_t^2 > k_{t0}^2 = 1\,\mathrm{GeV}^2$. The unintegrated gluon density $x\mathcal{A}(x, k_t^2, \mu^2)$ therefore is normalized to the MRST function when integrated up to k_{t0}^2.

In Fig. 2 we show a comparison of the gluon density distributions at $\mu^2 = 100\,\mathrm{GeV}^2$ obtained from JB, JS and

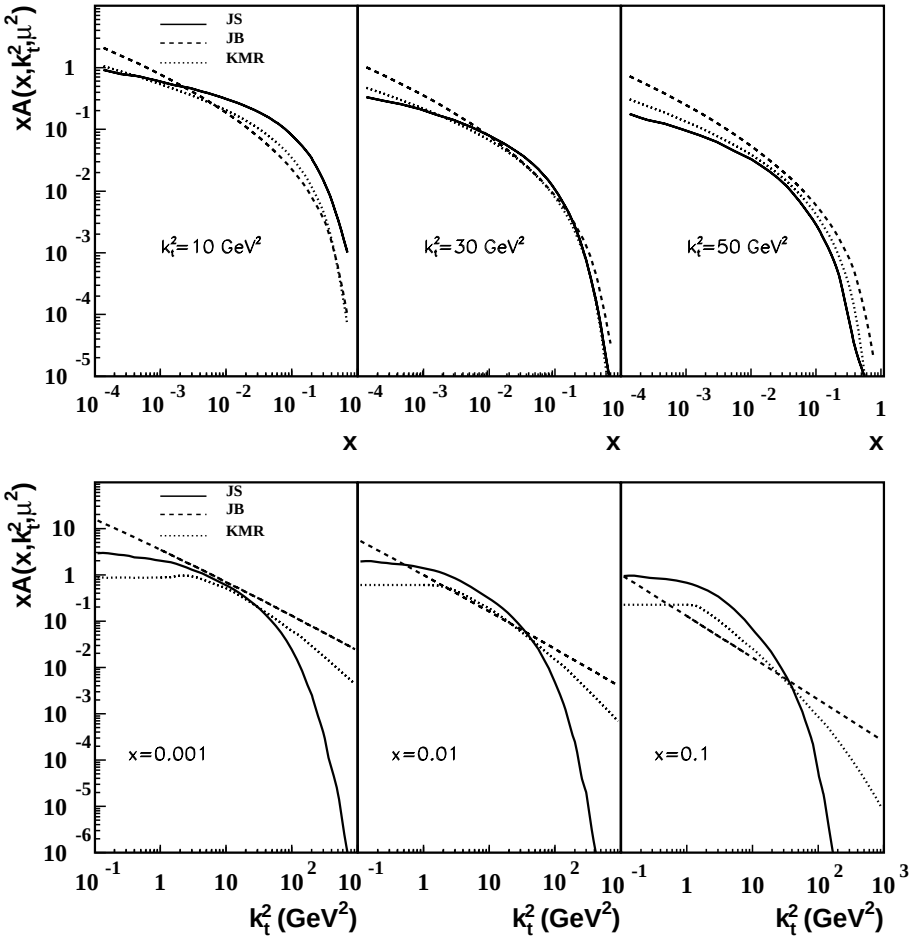

Fig. 2. The $k_{\rm t}$ dependent (unintegrated) gluon density at $\mu^2 = 100$ GeV^2 as a function of x for different values of $k_{\rm t}^2$ (upper part) and as a function of $k_{\rm t}^2$ for different values of x (lower part) as given by JS [23,24] (solid line), JB [37] (dashed line) and KMR [38,42] (dotted line)

KMR as a function of x for different values of $k_{\rm t}^2$ and as a function of $k_{\rm t}^2$ for different values of x.

From Fig. 2 we see that all three unintegrated gluon distributions show a significantly different behavior as a function of x but even more as a function of $k_{\rm t}$. It will be interesting to see how this different behavior is reflected in the prediction of cross sections for experimentally observable quantities like charm production at HERA.

4 Numerical results and discussion

A comparison between model predictions and data in principle has to be made on hadron level, and only if it turns out that hadronization effects are small will a comparison to parton-level predictions make sense. However, a full simulation even of the partonic final state, including the initial and final state QCD cascade needs a full Monte Carlo event generator. Such a Monte Carlo generator based on $k_{\rm t}$-factorization and using explicitly off-shell matrix elements for the hard scattering process convoluted with $k_{\rm t}$-unintegrated gluon densities is presently only offered by the CASCADE [23,24,36] program which uses the CCFM unintegrated gluon distribution. This is because only the CCFM evolution equation gives a description on how to explicitly build the initial state gluon radiation by applying angular ordering. Other sets of unintegrated gluon distribution can only be used to calculate quantities at the matrix element level, which can be compared to the data only if the effect of hadronization and of the complete initial state parton cascade are insignificant.

In the following we want to systematically compare the predictions from the $k_{\rm t}$-factorization approach to published data on charm production at HERA. For this we use D^* photo-production data from ZEUS [44] and D^* production in deep inelastic scattering from both ZEUS [45] and H1 [46]. To do this we first calculate observables using a pure parton-level calculation based on the matrix element calculation of BZ including the Peterson fragmentation function [47] for the transition from the charm quark to the observed D^* meson, where the D^* meson is assumed to take a momentum fraction z of the charm quark, in the $c\bar{c}$ center-of-mass (c.m.s.) frame. Then we compare the result with a full hadron level simulation using the Monte Carlo generator CASCADE with the matrix element of CE-CCH. Also here the Peterson fragmentation function is used but now with z being defined as the light-cone momentum fraction in the center-of-mass system of the string connecting the charm quark with its light quark partner, as implemented in JETSET/PYTHIA [48]. We choose the JS unintegrated gluon for this comparison, which is also

Table 2. Kinematic range of the different data used for comparison

ZEUS (γp) [44]	$130 < W < 280\,\text{GeV}$	$Q^2 < 1\,\text{GeV}^2$	$\lvert\eta\rvert < 1.5$	$p_\text{t} > 2\,\text{GeV}$
ZEUS DIS [45]	$0.02 < y < 0.7$	$1 < Q^2 < 600\,\text{GeV}^2$	$\lvert\eta\rvert < 1.5$	$1.5 < p_\text{t} < 15\,\text{GeV}$
H1 DIS [46]	$0.05 < y < 0.7$	$1 < Q^2 < 100\,\text{GeV}^2$	$\lvert\eta\rvert < 1.5$	$1.5 < p_\text{t} < 15\,\text{GeV}$

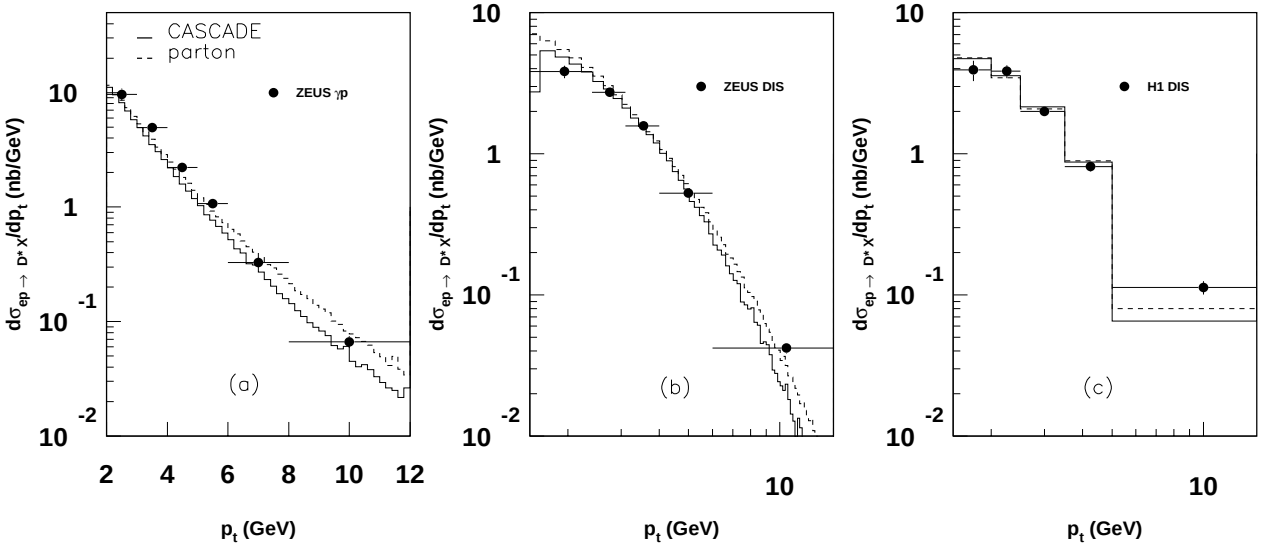

Fig. 3a–c. The differential cross section $\mathrm{d}\sigma/\mathrm{d}p_\text{t}$ for D^* production: **a** in photo-production (ZEUS [44]), **b** in DIS (ZEUS [45]) and **c** in DIS (H1 [46]). The solid line is the prediction from the full hadron level simulation CASCADE and the dashed line shows the parton-level calculation. In both cases the Peterson fragmentation function has been used

appropriate for a description of heavy quark production at high energies [28].

Next we investigate on parton level different unintegrated gluon densities. After the optimal choice of model parameters has been found for the JB gluon density, giving the best possible agreement with data, we show a comparison to the JS and KMR unintegrated gluon density. We then study the sensitivity of the model predictions to the details of the unintegrated gluon density, the charm mass and the scale.

We also consider the rapidity distribution of the produced D^*, which is very sensitive to the choice of the unintegrated gluon density and the details of the $c \to D^*$ fragmentation.

Then we investigate the x_γ distribution, which is sensitive to the details of the initial state cascade. We compare the predictions from a pure parton-level calculation and a full event simulation of CASCADE with the measurements.

At the end we show, motivated by preliminary studies of ZEUS [49], predictions which are sensitive to the details of the heavy quark production mechanism.

4.1 Transverse momentum distribution of D^* mesons: comparison of parton and hadron level

One observable which is expected to show only little sensitivity to the hadronization and to the full simulation of the initial and final state QCD cascades is the transverse momentum p_t of the D^* meson in photo-production and deep inelastic scattering. In Fig. 3 we show the transverse momentum distribution of D^* mesons as measured by the ZEUS [44, 45] and H1 [46] collaborations both in photo-production and deep inelastic scattering. The data are compared to the predictions of the CASCADE Monte Carlo event generator on hadron level including a full simulation of the partonic and hadronic final state. Also shown is the pure parton-level calculation using the matrix element of BZ. In both cases the transition from the charm quark to the observed D^* meson was performed by a simple Peterson fragmentation function (with $\epsilon = 0.06$ and a $c \to D^*$ branching ratio BR $= 0.26$). The scale $\bar{\mu}^2$ in $\alpha_\text{s}(\bar{\mu}^2)$ was set to $\bar{\mu}^2 = p_\text{t}^2 + m_c^2$ with p_t being the transverse momentum in the γg c.m.s. of the final charm quark state assuming $m_c = 1.5\,\text{GeV}$. The JS unintegrated gluon distribution [24] was used, with the scale μ (being related to the maximum angle) $\mu^2 \sim x_\gamma x_g s$. The sensitivity to the details of the charm fragmentation and to the full initial state gluon cascade simulation can be seen by comparing CASCADE with the parton-level calculation. We observe that the p_t distribution of D^* mesons both in photo-production and deep inelastic scattering is in general well described, both with the full hadron level simulation as implemented in CASCADE and also with the parton-level calculation supplemented with the Peterson fragmentation function. We can thus conclude that the p_t distribution is only little sensitive to the details of the charm fragmentation.

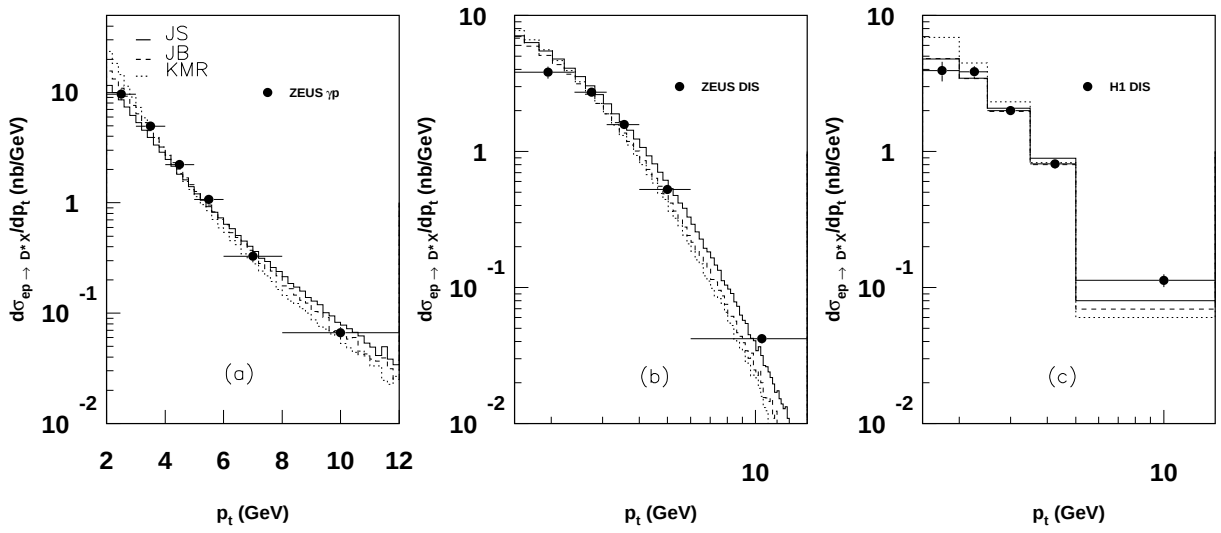

Fig. 4a–c. The differential cross section $\mathrm{d}\sigma/\mathrm{d}p_\mathrm{t}$ for D^* production: **a** in photo-production (ZEUS [44]), **b** in DIS (ZEUS [45]) and **c** in DIS (H1 [46]). The solid (dashed, dotted) line corresponds to using the JS (JB, KMR) unintegrated gluon density (all calculated at parton level). In all cases the Peterson fragmentation function has been used

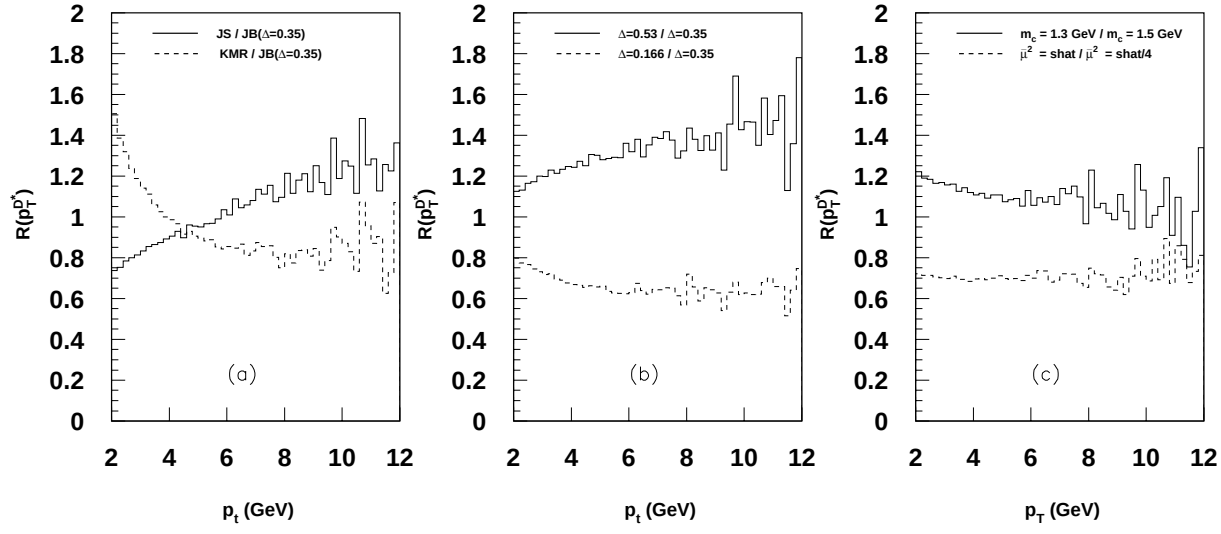

Fig. 5a–c. The ratio $R = (\mathrm{d}\sigma/\mathrm{d}p_\mathrm{t})/(\mathrm{d}\sigma^\mathrm{ref}/\mathrm{d}p_\mathrm{t})$ as a function of p_t for D^* photo-production. The reference set corresponds to the JB set with $\Delta = 0.35$, $m_c = 1.5\,\mathrm{GeV}$ and $\bar{\mu}^2 = \hat{s}/4$. In **a** the solid (dashed) line corresponds to the JS (KMR) unintegrated gluon distribution. In **b** the parameter Δ of the JB unintegrated gluon distribution is varied (the solid (dashed) line corresponds to $\Delta = 0.53$ (0.166)). In **c** the solid line corresponds to $m_c = 1.3\,\mathrm{GeV}$ and the dashed line to the setting $\bar{\mu}^2 = \hat{s}$

4.2 Transverse momentum distribution of D^* mesons: sensitivity to unintegrated gluon distributions

Since the transverse momentum distribution of D^* mesons is only slightly sensitive to the details of the full parton cascade and charm fragmentation, we can now proceed to investigate the sensitivity to the choice of the unintegrated gluon distribution. In Fig. 4 we show the prediction for $\mathrm{d}\sigma/\mathrm{d}p_\mathrm{t}$ obtained from the parton-level calculation as above using the JS, JB and KMR unintegrated gluon distributions in comparison with the data. Although differences are observed in the x_g and k_t distributions between the different unintegrated gluon distributions (see Fig. 2), it is interesting to note that very similar predictions for the D^* cross sections as a function of the transverse momentum p_t are obtained.

In Fig. 5 we investigate in more detail the different unintegrated gluon distributions, the effect of varying the Δ parameter (see Sect. 3) in the JB distribution and of changing the charm-quark mass and the evolution scale $\bar{\mu}$. The comparison is performed on the parton level and the Peterson fragmentation function has been used to produce the D^* meson. We define the ratio

$$R = \frac{\mathrm{d}\sigma/\mathrm{d}p_\mathrm{t}}{\mathrm{d}\sigma^\mathrm{ref}/\mathrm{d}p_\mathrm{t}},$$

where $\mathrm{d}\sigma^\mathrm{ref}/\mathrm{d}p_\mathrm{t}$ is calculated using $\Delta = 0.35$, $m_c = 1.5$ GeV and $\bar{\mu}^2 = \hat{s}/4$.

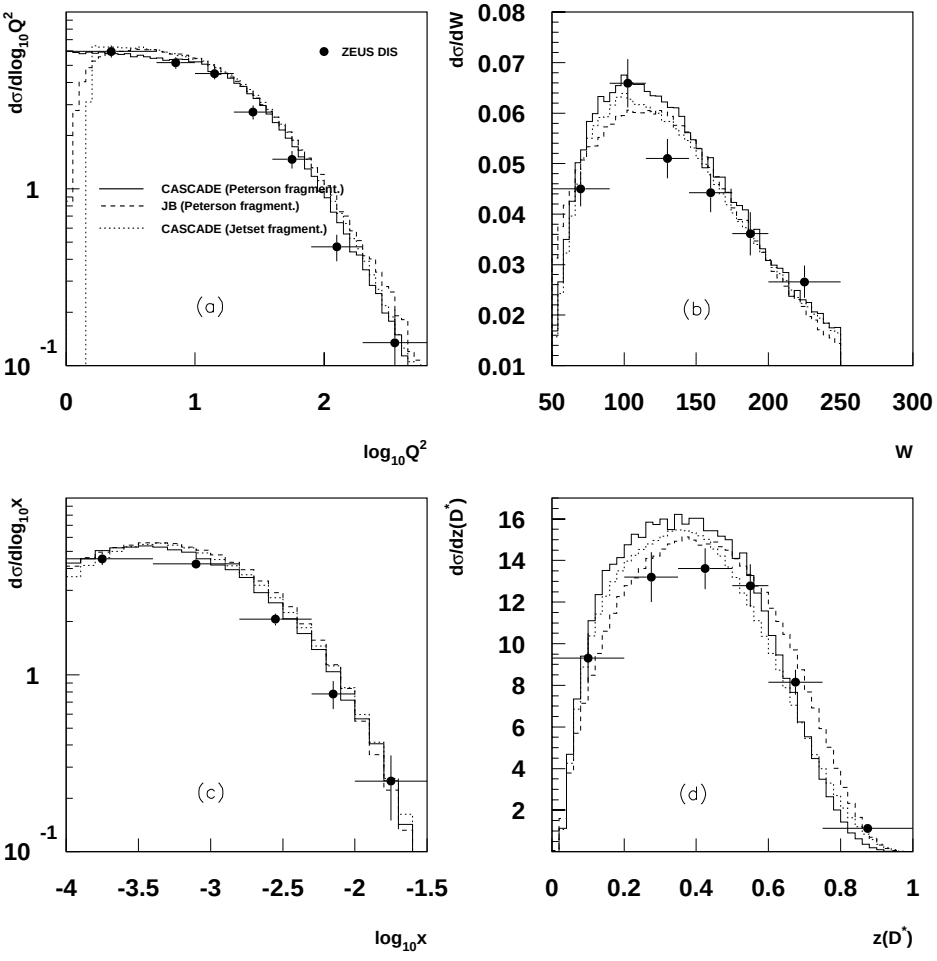

Fig. 6a–d. Differential cross sections as measured by ZEUS. Shown is a comparison of the calculations using CASCADE with the JS (solid line) and JB (dashed line) unintegrated gluon density. The dotted line shows the CASCADE prediction using the JETSET/PYTHIA charm fragmentation function

The ratio of the differential cross section as a function of p_t obtained from the parton-level calculation supplemented with the Peterson fragmentation function using the JS (solid line) and KMR (dashed line) unintegrated gluon distributions is shown in Fig. 5a. The fact that the ratios show a different behavior is directly connected to the different slopes in the k_t distribution of the parton densities (see Fig. 2).

In Fig. 5b we show the ratio R for different values of the Δ parameter of the JB unintegrated gluon distribution. We observe that the ratio R varies with p_t in the low p_t-range but seems to flatten off at higher p_t. For Δ-values larger than the reference value an increase in R is observed, whereas Δ-values below the reference value result in a decreasing R. This implies that the p_t spectra get harder with increasing Δ-values and softer with decreasing Δ-values compared to the reference value $\Delta = 0.35$ [20].

In Fig. 5c the effects of changing the mass of the charm quark and the evolution scale are illustrated. A decrease of the charm-quark mass leads to an increase of the ratio R in the low p_t-range whereas an increase of the interaction scale from $\bar{\mu}^2 = \hat{s}/4$ to $\bar{\mu}^2 = \hat{s}$ leads to an overall decrease of R by 20–25%.

4.3 Inclusive distribution: comparison of parton and hadron level

In Fig. 6 we compare the measured cross section for D^* production as function of Q^2, W, x_{Bj} and z_D with calculations using CASCADE with the JS unintegrated gluon distribution (solid line) and the parton-level calculation supplemented with the Peterson fragmentation function using the JB unintegrated gluon density (dashed line). We also show the effect of changing the charm fragmentation (dotted line).

Good agreement with the data is observed for both CASCADE with the JS unintegrated gluon density as well as for the parton-level calculation with the JB ($\Delta = 0.35$) unintegrated gluon density in the differential cross sections as a function of $\log Q^2$ and $\log x_{\mathrm{Bj}}$ [22]. The differential cross section as a function of W, as shown in Fig. 6b, is well described by CASCADE and somewhat less well described by JB in the peak region, although the errors of the measurement are fairly large. For the energy fraction z_D taken by the D^* meson, presented in Fig. 6d, we observe a slight shift of the JB distribution towards higher z_D-values compared to CASCADE. However, the z_D distribution is sensitive to the details of the D^* fragmentation, which is indicated by the dotted line in Fig. 6d, which represents

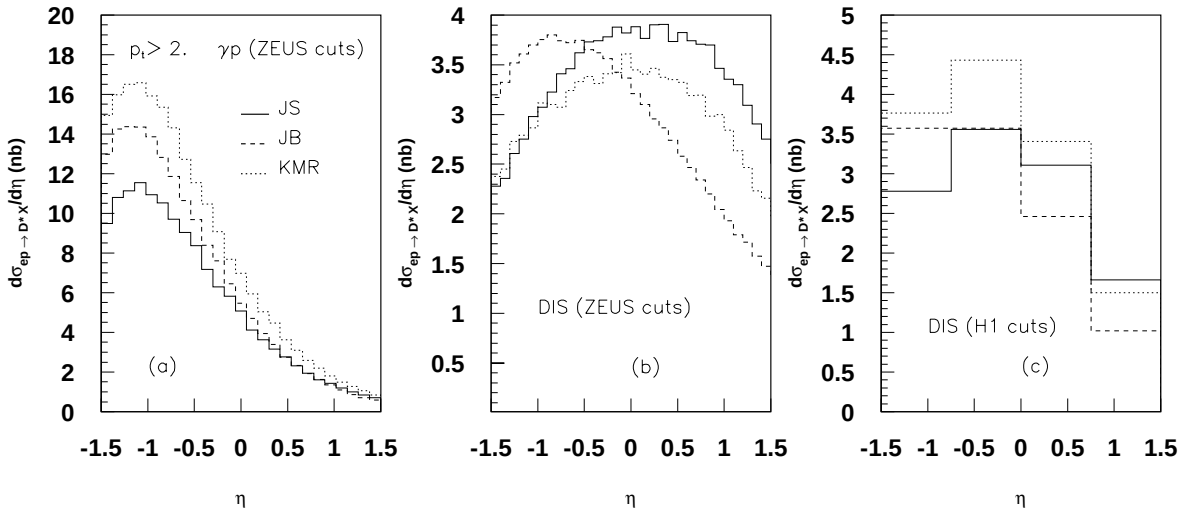

Fig. 7a–c. The differential cross section $d\sigma/d\eta$ for D^* production: **a** in photo-production (ZEUS cuts), **b** in DIS (ZEUS cuts) and **c** in DIS (H1 cuts). Shown is a comparison of the calculations using the JS (solid line), JB (dashed line) and KMR (dotted line) unintegrated gluon density

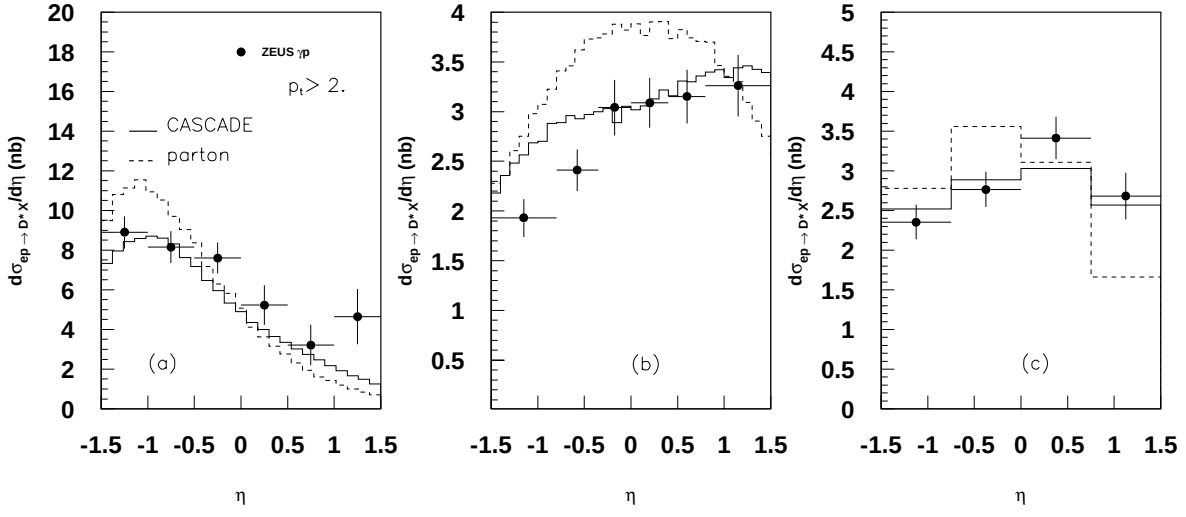

Fig. 8a–c. The differential cross section $d\sigma/d\eta$ for D^* for **a** photo-production as measured by ZEUS [44], **b** DIS from ZEUS [45] and **c** DIS from H1 [46]. The histograms show the full hadron level simulation from CASCADE (solid line) compared to the parton-level calculation (dashed line), both using the JS unintegrated gluon density

CASCADE, but using the JETSET/PYTHIA fragmentation function instead of the Peterson one. In conclusion of the above comparisons, we observe a good description of the differential cross sections as a function of the transverse momentum p_t of the D^* meson as well as of inclusive quantities: the unintegrated gluon distributions which have been considered are reasonable for the description of the data.

4.4 Rapidity distribution of D^* mesons: comparison of parton and hadron level

In photo-production and in DIS the differential cross section $d\sigma/d\eta$, where η is the pseudo-rapidity of the D^* meson, is sensitive to the choice of the unintegrated gluon distribution. In Fig. 7 we show a comparison of $d\sigma/d\eta$ in γp and in DIS at parton level supplemented with the Peterson fragmentation function using the JS (solid line), JB (dashed line) and the KMR (dotted line) unintegrated gluon distribution. Large differences in $d\sigma/d\eta$ are visible, but one has to keep in mind that especially the η distribution is also sensitive to the details of the $c \to D^*$ fragmentation, and therefore a clear distinction of the unintegrated gluon distributions based on this quantity alone might be questionable. In Fig. 8 we show $d\sigma/d\eta$, in photo-production and in DIS, using the JS unintegrated gluon distribution at parton level and with the full simulation of CASCADE. We observe that the parton-level prediction including the Peterson fragmentation function is not able to describe the measurements over the full range of η. The effect of a full hadron level simulation is clearly visible as CASCADE provides a much better description of the ex-

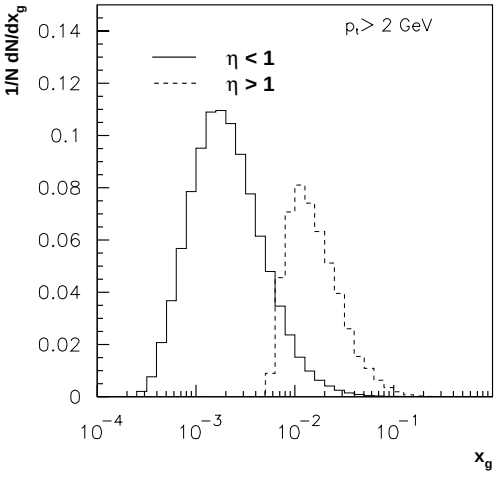

Fig. 9. The distribution of x_g in D^* photo-production for $\eta < 1$ and $\eta > 1$ for $p_{\mathrm{t}D^*} > 2\,\mathrm{GeV}$

perimental data. Here the JETSET/PYTHIA charm fragmentation has been used.

From the above it is obvious that the η distribution is sensitive to the details of the fragmentation of the charm quark into the D^* meson but also sensitive to the simulation of the initial state QCD cascade. It also shows that an ordinary next-to-leading calculation at parton level cannot be expected to describe the η distribution, since a full simulation of the initial state parton evolution obviously is important for a reasonable description of heavy quark decays. However, in photo-production even the full event simulation of CASCADE shows differences to the measurement at large values of $\eta > 1$. These large values of $\eta > 1$ are related to large values of the momentum fraction $x_g \gtrsim 0.03$ of the gluons entering the hard subprocess, as shown in Fig. 9. It is intuitively understandable that the small-x approximation becomes less reliable at large x_g-values. In addition, values of $x_g \gtrsim 0.03$ are not constrained in the determination of JS as described in [24, 28]. It is therefore not surprising that the description is not perfect in this kinematic region.

In Fig. 10 we show the cross section $\mathrm{d}\sigma/\mathrm{d}\eta$ of deep inelastic D^* production as measured by H1 [46] for different ranges in z_D together with the prediction of CASCADE with the JETSET/PYTHIA charm fragmentation function and the JS unintegrated gluon density (solid line). Also shown is the parton-level calculation supplemented with the Peterson fragmentation function and the JB (dashed line) unintegrated gluon density. We observe that again the JS unintegrated gluon distribution together with a full event simulation gives a reasonable description of the data of this double differential cross section.

4.5 D^* and associated jet production: comparison of parton and hadron level

In the BFKL and/or CCFM equations the transverse momenta of the exchanged or emitted partons are only restricted by kinematics. In such a scenario, the hardest p_{t} emission can be anywhere in the gluon chain, and does not need to sit closest to the photon as required by the strong q^2 ordering in DGLAP.

Photo-production of charm is an ideal testing ground for studying the underlying parton dynamics, since charm quarks are predominantly produced via $\gamma \to c\bar{c}$. The observation of any emission (jet) with $p_{\mathrm{t}} > p_{\mathrm{t}}^c$ ($p_{\mathrm{t}}^{\bar{c}}$) indicates a scenario which in DGLAP is possible only in a full $O(\alpha_{\mathrm{s}}^2)$ calculation or when charm excitation of the photon is included. However, in k_{t}-factorization such a scenario comes naturally, since the transverse momenta along the evolution chain are not k_{t} ordered.

The ZEUS collaboration has measured charm and associated jet production [44]. In these measurements, the quantity of interest is the fractional photon momentum involved in the production of the two jets of highest E_{t}, which is experimentally defined by

$$x_\gamma^{\mathrm{OBS}} = \frac{E_{1\mathrm{t}} \exp(-\eta_1) + E_{2\mathrm{t}} \exp(-\eta_2)}{2E_e y}, \qquad (10)$$

with $E_{i\mathrm{t}}$ and η_i being the transverse energy and rapidity of the hardest jets and y being the fractional photon energy. In Fig. 11 we show a diagrammatic representation of the different processes involved in charm photo-production. Thus, if the two hardest transverse momentum jets are produced by the $c\bar{c}$ pair, then x_γ^{OBS} is close to unity (Fig. 11a), but if a gluon from the initial state cascade together with one of the c quarks form the hardest transverse momentum jets, then $x_\gamma^{\mathrm{OBS}} < 1$ (Fig. 11b). In a leading-order calculation using the collinear approximation $x_\gamma^{\mathrm{OBS}} < 1$ indicates a resolved photon-like process (Fig. 11b). Such a scenario is obtained naturally also in a full NLO ($\mathcal{O}(\alpha_{\mathrm{s}}^2)$) calculation, because in the three parton final state ($c\bar{c}g$) any of these partons are allowed to take any kinematically accessible value (Fig. 11c). In the k_{t}-factorization approach the anomalous component of the photon ($\gamma \to c\bar{c}$) is automatically included, since there is no restriction on the transverse momenta along the evolution chain.

The experimentally observed x_γ^{OBS} spectrum (Fig. 12c) shows a tail to small values of x_γ^{OBS}, indicating that the hardest emission is indeed not always coming from the charm quarks. In Fig. 12a we show a comparison of the x_γ^{OBS} distribution obtained on parton level with the JB unintegrated gluon density. Indicated is also the contribution from events where the gluon is the hardest, next-to-hardest and softest parton. A significant part of the cross section comes from events where the gluon is the jet with the largest transverse momentum [25]. In Fig. 12b we compare the x_γ^{OBS} distribution obtained at parton level from the JB unintegrated gluon with the one from JS. In both cases a significant tail towards small x_γ-values is observed, however the details depend on the unintegrated gluon distribution. In Fig. 12c we show a comparison of the measurement from the ZEUS collaboration [44] with the prediction from the full event simulation of CASCADE using the JS unintegrated gluon distribution and applying jet reconstruction and jet selection at the hadron level. We observe a reasonably good agreement, showing

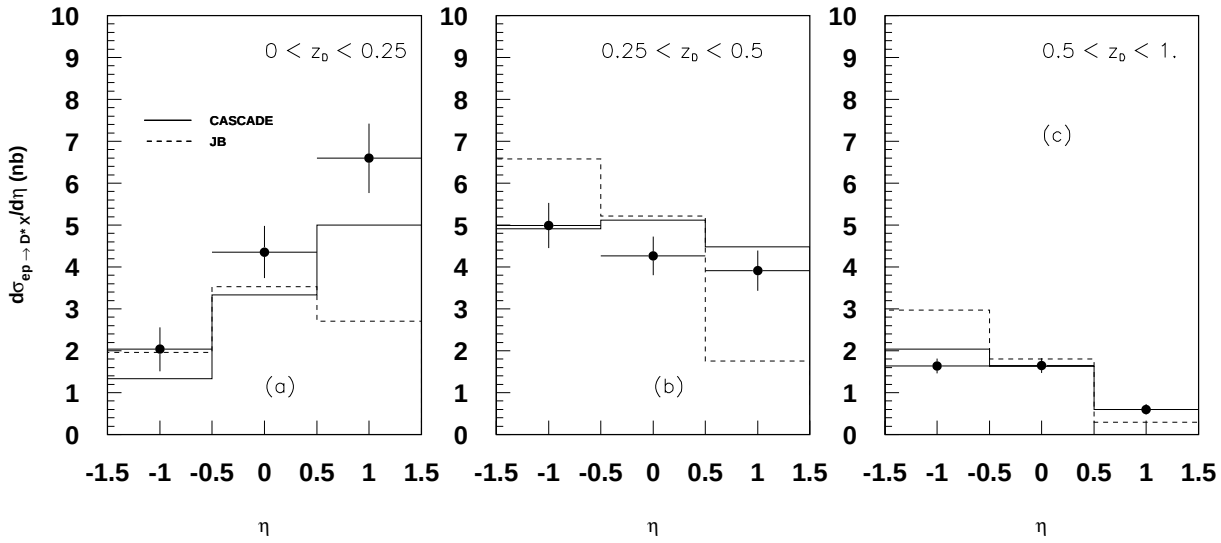

Fig. 10a–c. The differential cross section $\mathrm{d}\sigma/\mathrm{d}\eta$ for D^* production in three bins of z_D as measured by H1 [46]. The data are compared to the calculations using CASCADE with the JETSET/PYTHIA charm fragmentation and with the JS (solid line) unintegrated gluon density. The dashed line shows the parton-level calculation with the Peterson charm fragmentation function and with the JB unintegrated gluon density

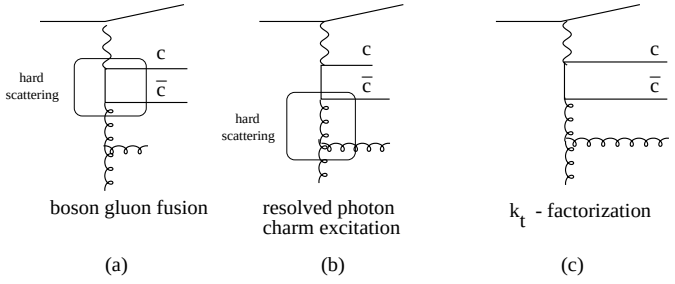

Fig. 11a–c. Diagrammatic representation of the processes involved in charm photo-production. **a** shows the typical boson–gluon fusion diagram; the hard partons are the $c\bar{c}$ quarks. **b** shows a typical resolved photon (charm excitation) diagram; the hard partons are here the $\bar{c}g$. **c** shows a typical diagram in k_t-factorization; any two of $c\bar{c}g$ can be the hardest partons

indeed a large tail towards small x_γ^{OBS}-values in agreement with the observation from the data. We can conclude that the k_t-factorization approach effectively simulates heavy quark excitation and indeed the hardest p_t emission comes frequently from a gluon in the initial state gluon cascade.

Another interesting quantity is the angular distribution of resolved photon-like events ($x_\gamma^{\mathrm{OBS}} < 0.75$) compared to the direct photon-like events ($x_\gamma^{\mathrm{OBS}} > 0.75$) [49, 50]. An important difference between the two (direct (Fig. 11a), resolved (Fig. 11b)) scattering processes is that a quark (charm in this case) is the propagator of the hard scattering in the direct photon-like events and a gluon in the dominant resolved photon-like events. The angular distribution of dijets with a $D^{*\pm}$ in the final state is dependent on the type of propagator (quark or gluon) connecting both jets (if we neglect the case where a parton is emitted in the rapidity range between the two hardest jets). In the collinear approximation, the angular distribution is determined by the matrix element ($\gamma g \to c\bar{c}$ in the direct case or $cg \to cg$ in the resolved photon case). In the k_t-factorization approach the angular distribution will be determined from the off-shell matrix element, which covers both scattering processes.

In Fig. 13 we show the $|\cos\theta^*|$ distribution, where θ^* is the scattering angle of the hard jets to the beam axis in the dijet c.m.s. Applying the same cuts and using the same jet-algorithm as in [49, 50], we can see that the direct photon-like events give a slow increase in cross section with increasing $|\cos\theta^*|$. However, the cross section of the resolved photon-like events increases very rapidly because of the t-channel gluon exchange being a combined effect of the off-shell gluon and the unintegrated gluon distribution.

Thus the partons of the initial state radiation in the k_t-factorization approach give information on the spins of the propagators, as well as on the parton dynamics of the underlying sub-processes. We specifically checked the dynamics in our approach by only allowing the final state partons ($c\bar{c}$) to appear in the hard scattering (i.e. turning off the simulation of the initial state gluon cascade in CASCADE, but keeping the final state parton shower). Here we should expect to see only the quark exchange kind of behavior for both direct and resolved like events, which is also verified as seen in Fig. 13 with dotted and dashed lines overlapping around the default mode with $x_\gamma > 0.75$.

In order to further probe the parton dynamics in this approach, we divide the entire sample into two parts, one where the D^* proceeds along the photon direction (i.e. $\eta_{D^*} < 0$) and one where it travels along the proton direction (i.e. $\eta_{D^*} > 0$). If the t-channel gluon is indeed the dominant contribution to the cross section, then the angular distribution will be peaked towards the direction of the incoming photon. This asymmetry should persist (more or less) equally for charm and anticharm. Such an asymmetry cannot be seen in the inclusive dijet sample

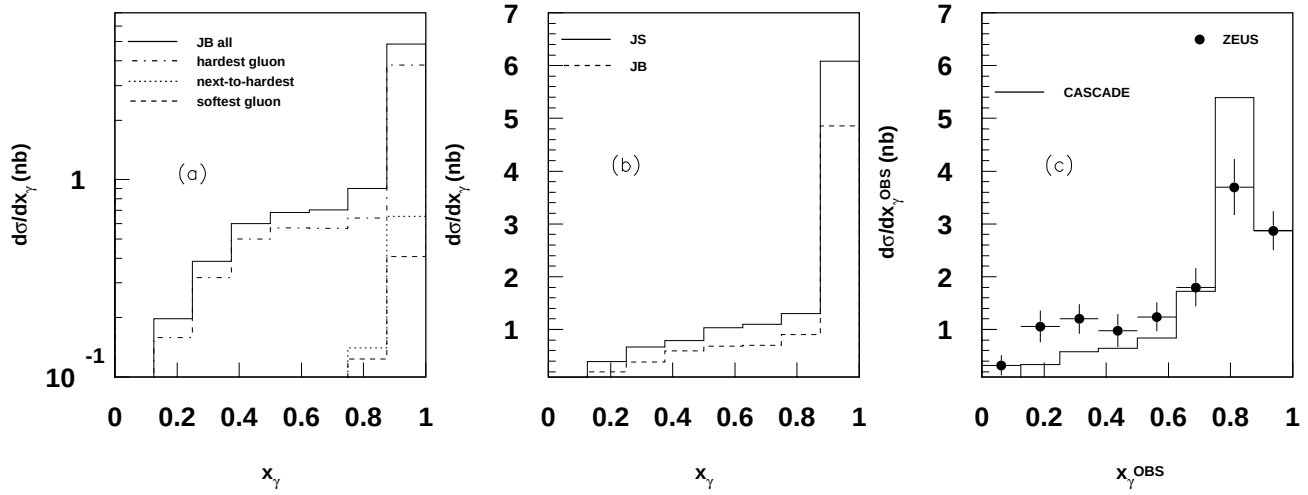

Fig. 12a–c. The differential cross section $\mathrm{d}\sigma/\mathrm{d}x_\gamma$ for $Q^2 < 1\,\mathrm{GeV}^2$. In **a** the parton-level calculation is shown using the JB unintegrated gluon density (solid line). Shown are also the contributions where the gluon takes the largest (dash-dotted line), next-to-largest (dashed line) and smallest (dotted line) transverse momentum. In **b** the JB (solid line) and JS (dashed line) sets are used in the parton-level calculation. In **c** the measurement of ZEUS [44] is compared to the full event simulation obtained from CASCADE using the JS unintegrated gluon distribution

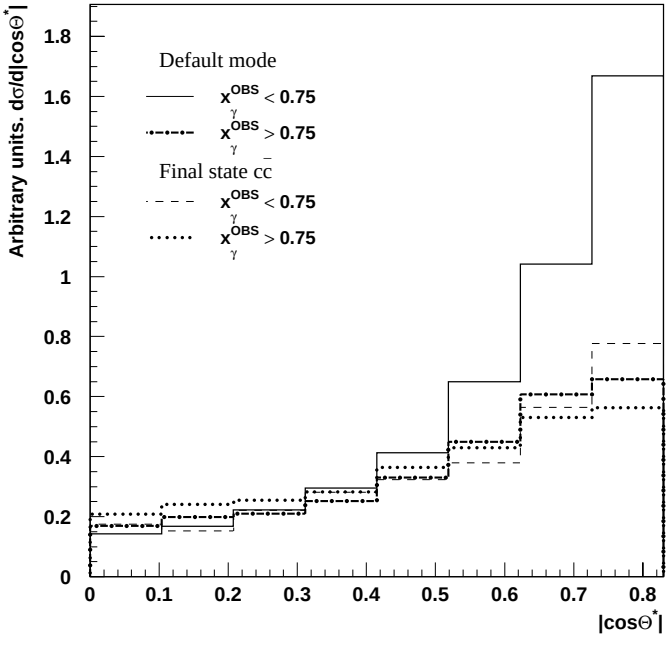

Fig. 13. The distribution in $|\cos\theta^*|$ for resolved photon-like events ($x_\gamma^{\mathrm{OBS}} < 0.75$) and for direct photon-like events ($x_\gamma^{\mathrm{OBS}} > 0.75$) within the kinematic range of the ZEUS measurement [49]

(without separation of gluon and quark jets), because by definition the distribution must be $t \leftrightarrow u$ symmetric as long as we do not attempt to discriminate different kinds of jets.

In Fig. 14 we show the $|\cos\theta^*|$ distribution for the two cases with the D^* found in the photon (a) and proton (b) direction, with $x_\gamma^{\mathrm{OBS}} > 0.75$ and $x_\gamma^{\mathrm{OBS}} < 0.75$ in the same phase space as in [49,50], except for an additional cut on the average pseudo-rapidity of the jets, $|\overline{\eta}| < 0.1$, to ensure an unbiased phase space region as discussed in [51]. As one can see, with the D^* in the photon direction, there is a steep rise in the cross section for resolved photon-like events compared to the direct photon-like events. This increase in $|\cos\theta^*|$ obtained through the initial state gluon cascade in the k_{t}-factorization approach can also be interpreted as "charm excitation" processes. On the other hand, with the D^* in the proton direction, we can only see a mild increase in cross section for both direct and resolved photon-like events, which shows that the quark exchange is the dominant contribution (in the HERA kinematic range).

5 Conclusion

Three different models based on small x resummation (BFKL and CCFM formalism) and k_{t}-factorization have been studied in various aspects. Two of the approaches only deliver results on the parton level (JB and KMR) whereas the third one (JS) has been implemented into an event generator providing complete simulation of the initial and final state parton shower and hadronization. The ability of the models to reproduce the experimental data has been investigated for charm production in the kinematic range of HERA. The aim has been to find out whether optimal sets of model parameters could be found leading to a satisfactory description of all data, but also to illustrate the sensitivity of the model prediction from variations of the various parameters. The unintegrated gluon distributions of the three approaches exhibit different behaviors as a function of x but especially as a function of k_{t}. In spite of this we find good agreement between the models and data on p_{t}, $\log Q^2$, $\log W$ and $\log x_{\mathrm{Bj}}$ distributions, which indicates that these variables are not sensitive enough to differentiate between the models. The poorer

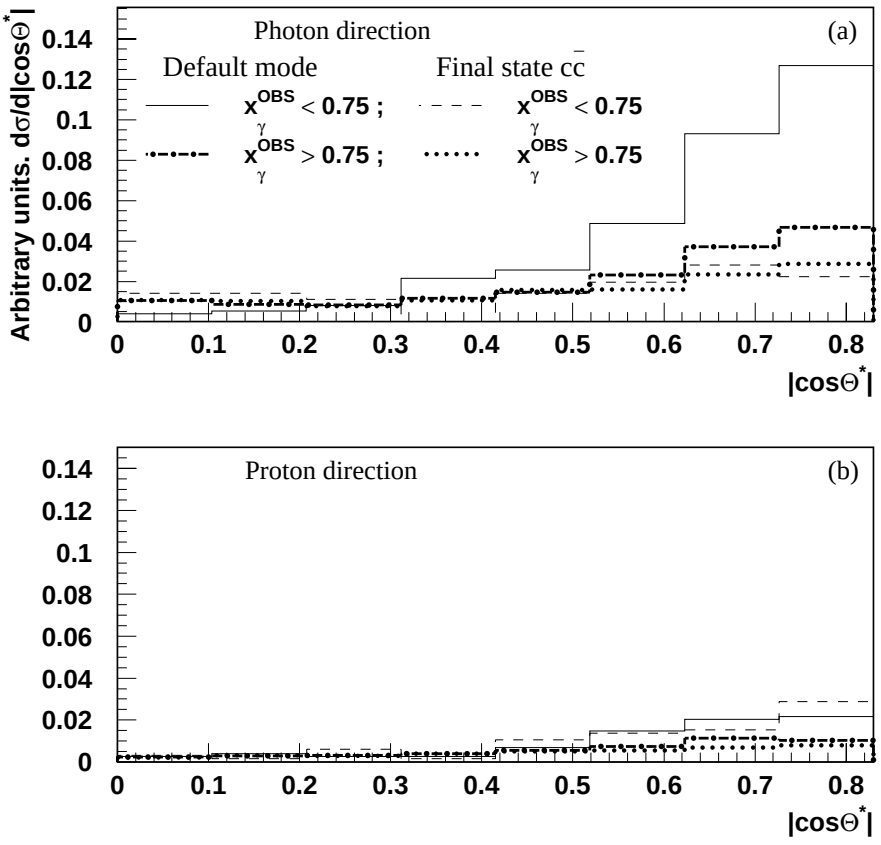

Fig. 14a,b. $|\cos\theta^*|$ distribution with $\eta_{D^*} < 0$ **a** (photon direction) and $\eta_{D^*} > 0$ **b** (proton direction) within the kinematic range of the ZEUS measurement [49, 50]

description of the z_D distribution observed for two of the models might be due to a different treatment of the D^* fragmentation. The sensitivity to the D^* fragmentation is seen very clearly in the case of the η distribution which also needs a full simulation of the initial and final state parton emission to give a reasonable description of the data.

From comparisons with the data on photo-production of charm leading to jets, it became evident that a gluon from the initial cascade frequently produces the jet of highest p_t. Considering the uncertainties due to parton radiation and hadronization effects the models give consistent results. The distribution in polar angle of the hard jets, as generated by the CASCADE program, predicts that the gluon propagator is dominant in the hard scattering of resolved photon-like events, leading to high p_t-jets initiated by a quark and a gluon. The polar angle spectrum for direct photon events, however, is consistent with the propagator of the hard scattering being a quark, resulting in hard quark–antiquark jets.

We have shown that the k_t-factorization approach can be consistently used to describe measurements of charm production at HERA, which are known to be not well reproduced in the collinear approach. We have also shown that in k_t-factorization, resolved photon-like processes are effectively simulated including the proper angular distributions. The k_t-factorization approach has now become a challenging tool to understand the underlying dynamical processes in high energy collisions.

Acknowledgements. We are grateful to M. Derrick for careful reading of the manuscript. S.B. and N.Z. thank the Royal Swedish Academy of Science for support. N.Z. was supported in part by Grant RFFI 02-02-17513. One of us (S.P.) acknowledges the support by Natural Sciences and Engineering Research Council of Canada (NSERC) and thanks M. Drees, U. Karshon and M. Wing for valuable discussions. H.J. wants to thank the DESY directorate for hospitality and support.

References

1. L. Gribov, E. Levin, M. Ryskin, Phys. Rep. **100**, 1 (1983)
2. J. Collins, R. Ellis, Nucl. Phys. B **360**, 3 (1991)
3. S. Catani, M. Ciafaloni, F. Hautmann, Nucl. Phys. B **366**, 135 (1991)
4. E. Kuraev, L. Lipatov, V. Fadin, Sov. Phys. JETP **44**, 443 (1976)
5. E. Kuraev, L. Lipatov, V. Fadin, Sov. Phys. JETP **45**, 199 (1977)
6. Y. Balitskii, L. Lipatov, Sov. J. Nucl. Phys. **28**, 822 (1978)
7. M. Ciafaloni, Nucl. Phys. B **296**, 49 (1988)
8. S. Catani, F. Fiorani, G. Marchesini, Phys. Lett. B **234**, 339 (1990)
9. S. Catani, F. Fiorani, G. Marchesini, Nucl. Phys. B **336**, 18 (1990)
10. G. Marchesini, Nucl. Phys. B **445**, 49 (1995)
11. V. Gribov, L. Lipatov, Sov. J. Nucl. Phys. **15**, 438, 675 (1972)
12. L. Lipatov, Sov. J. Nucl. Phys. **20**, 94 (1975)
13. G. Altarelli, G. Parisi, Nucl. Phys. B **126**, 298 (1977)

14. Y. Dokshitser, Sov. Phys. JETP 4**6**, 641 (1977)
15. E. Levin, M. Ryskin, Y. Shabelskii, A. Shuvaev, Sov. J. Nucl. Phys. **53**, 657 (1991)
16. E. Levin, M. Ryskin, Y. Shabelskii, A. Shuvaev, Sov. J. Nucl. Phys. **54**, 867 (1991)
17. M. Ryskin, Y. Shabelskii, A. Shuvaev, Z. Phys. C **69**, 269 (1996), hep-ph/9506338
18. A. Lipatov, N. Zotov, Mod. Phys. Lett. A **15**, 695 (2000)
19. A. Lipatov, V. Saleev, N. Zotov, Mod. Phys. Lett. A **15**, 1727 (2000), hep-ph/0008283
20. S. Baranov, N. Zotov, Phys. Lett. B **458**, 389 (1999)
21. S. Baranov, H. Jung, N. Zotov, Charm production in the semi-hard approach of QCD, in Proceedings of the Workshop on Monte Carlo generators for HERA physics, edited by A. Doyle, G. Grindhammer, G. Ingelman, H. Jung (DESY, Hamburg, 1999), p. 484, hep-ph/9910210
22. S. Baranov, H. Jung, N. Zotov, Nucl. Phys. Proc. Suppl. **99**, 192 (2000), hep-ph/0011127
23. H. Jung, CCFM prediction on forward jets and F_2: parton-level predictions and a new hadron level Monte Carlo generator Cascade, in Proceedings of the Workshop on Monte Carlo generators for HERA physics, edited by A. Doyle, G. Grindhammer, G. Ingelman, H. Jung (DESY, Hamburg, 1999), p. 75, hep-ph/9908497
24. H. Jung, G. Salam, Eur. Phys. J. C **19**, 351 (2001), hep-ph/0012143
25. S. Baranov, N. Zotov, Phys. Lett. B **491**, 111 (2000)
26. S. Baranov, M. Smižanská, Phys. Rev. D **62**, 014012 (2000)
27. P. Hägler et al., Phys. Rev. D **62**, 071502 (2000)
28. H. Jung, Phys. Rev. D **65**, 034015 (2002), DESY-01-136, hep-ph/0110034
29. P. Hägler et al., Phys. Rev. D **63**, 077501 (2001), hep-ph/008316
30. P. Hägler et al., Phys. Rev. Lett. **86**, 1446 (2001), hep-ph/0004263
31. F. Yuan, K.-T. Chao, Phys. Rev. D **63**, 034006 (2001), hep-ph/0008302
32. F. Yuan, K.-T. Chao, Phys. Rev. Lett. **87**, 022002 (2001)
33. V. Saleev, N. Zotov, Mod. Phys. Lett. A **11**, 25 (1996)
34. R. Prange, Phys. Rev. **110**, 240 (1958)
35. G.P. Lepage, J. Comp. Phys. **27**, 192 (1978), CLNS-80/447
36. H. Jung, Comp. Phys. Comm. **143**, 100 (2002), hep-ph/0109102, DESY 01-114, http://www.quark.lu.se/ hannes/cascade/
37. J. Blümlein, On the k_t dependent gluon density of the proton, in Proceedings of the Workshop on Deep Inelastic Scattering and QCD, edited by J. Laporte, Y. Sirois (1995), DESY 95-121
38. M.A. Kimber, A.D. Martin, M.G. Ryskin, Phys. Rev. D **63**, 114027 (2001)
39. M. Glück, E. Reya, A. Vogt, Z. Phys. C **67**, 433 (1995)
40. V.S. Fadin, L.N. Lipatov, Phys. Lett. B **429**, 127 (1998)
41. J. Kwiecinski, A. Martin, A. Stasto, Phys. Rev. D **56**, 3991 (1997)
42. M. Kimber, Extrapolation of unintegrated gluon density, private communication
43. A.D. Martin, R.G. Roberts, W.J. Stirling, R.S. Thorne, Nucl. Phys. Proc. Suppl. **79**, 105 (1999), hep-ph/9906231
44. ZEUS Collaboration, J. Breitweg et al., Eur. Phys. J. C **6**, 67 (1999)
45. ZEUS Collaboration, J. Breitweg et al., Eur. Phys. J. C **12**, 35 (1999), DESY 99-101
46. H1 Collaboration, C. Adloff et al., Phys. Lett. B **528**, 199 (2002), hep-ex/0108039
47. C. Peterson, D. Schlatter, I. Schmitt, P.M. Zerwas, Phys. Rev. D **27**, 105 (1983)
48. T. Sjostrand et al., Comput. Phys. Commun. **135**, 238 (2001), hep-ph/0010017
49. ZEUS Collaboration, Dijet angular distributions in D^* photoproduction at HERA, contributed paper 499 to HEP, Budapest, Hungary, July 12–18, 2001
50. S. Padhi, Heavy-Flavoured Jets at HERA, hep-ex/0111023
51. S. Padhi, Ph.D. thesis (in preparation), McGill University, Canada, 2002